Chemical Engineering Journal 97 (2004) 11–25

Chemical Engineering Journal

www.elsevier.com/locate/cej

Acoustic emission measurement of low velocity plunging jets to monitor bubble size

Jonathan W.R. Boyd, Julie Varley*

Department of Chemical Engineering and Chemical Technology, Imperial College of Science, Technology and Medicine, Prince Consort Road, London SW7 2BY, UK

Received 26 October 2002; accepted 5 April 2003

Abstract

Acoustic emission measurement is a possible method for non-invasive, real-time process monitoring. The monitoring of acoustic emissions from a laboratory scale plunging jet at low velocities has been shown to allow identification of the onset of air entrainment, differentiate between certain types of hydrodynamic regime. The acoustic technique has been used to measure the variation of average bubble size and bubble size distribution with jet flow rate and nozzle height. NaCl and xanthan gum solutions have been used to demonstrate the effects of coalescence repression and viscosity respectively on variation of bubble size with jet flow rate and nozzle height.

Keywords: Plunging jet; Acoustic emission; Process monitoring

1. Introduction

The plunging jet is used as a means of entraining air into a liquid in a variety of industrial processes. In particular, in wastewater treatment it is considered to be an efficient means of oxygenating activated sludge [1]. The advantages of a plunging jet as a means of aeration are that the process is simple, no air compressor is required and there is no clogging of diffusers. There are other processes that involve plunging jets such as the pouring of molten glass and metals, plastics or foods and in these cases bubble formation and entrainment is undesirable.

Bin [1] has summarised the bubble dispersion characteristics of plunging jets. A bubble dispersion, which is the result of a plunging jet, is divided into two distinctly different regions: a conical biphasic region comprised of fine primary bubbles (<1 mm in diameter) formed by the high turbulent intensity which penetrate to a maximum depth; and a region of larger rising bubbles formed from coalescence that surrounds the biphasic region (secondary bubbles). In previous studies, photography has been used to measure the bubble size distributions; however, generally only secondary bubbles are measured. In general for air–water systems, secondary bubbles measured have a distribution with a Sauter mean diameter of 3–4 mm. The mean diameter is practically independent of jet velocity and nozzle height. The primary Sauter mean diameter of bubbles in the biphasic region has been measured to be 0.02–0.33 mm. The largest recorded bubbles in water had diameters of about 7 mm. Evans et al. [2] measured the bubble diameter distribution within the mixing zone of the dispersion and typically found a log-normal distribution, skewed towards the smaller bubble sizes. Evans et al. [2] occasionally also found bimodal distributions and it was proposed that the two distributions contributing arose from (i) primary bubbles generated by the plunging jet and (ii) bubbles generated by break-up of re-circulating larger bubbles within the mixing zone. Evans et al. [2] used the critical Weber number, which was defined on the basis of the energy dissipation rate per unit volume in the mixing zone, to determine the maximum bubble diameter as:

$$d_{\mathrm{b,max}} = (\tfrac{1}{2} We_{\mathrm{c}} \sigma)^{3/5} \rho_{\mathrm{L}}^{-1/5} E^{-2/5} \quad (1)$$

where We_{c} is the critical Weber number, σ the surface tension, ρ_{L} the liquid density and E is the energy dissipation defined by:

$$E \cong \frac{\rho_{\mathrm{L}} b v_j^3}{2 L_{\mathrm{mz}}} (1 - 2b) \quad (2)$$

where v_j is the jet velocity, b the jet/column cross sectional area and L_{mz} is the mixing zone length. The Sauter mean diameter was found to be $0.61 d_{\mathrm{b,max}}$. Eq. (1) assumes

* Corresponding author. Tel.: +44-207-594-5698; fax: +44-207-594-5629.
E-mail address: j.varley@ic.ac.uk (J. Varley).

1385-8947/$ – see front matter
doi:10.1016/S1385-8947(03)00115-3

that only bubble break-up occurs in the dispersion with no coalescence.

McKeogh and Ervine [3] described three types of bubble dispersions, which result from plunging jets. A type 1 dispersion occurs at low nozzle heights where the surface of the water jet is smooth and many small bubbles are formed, which are subsequently dispersed throughout the mixing vessel. Type 3 dispersions occur when the surface of the jet is rough and turbulent; producing relatively large bubbles, which are formed in the localised region of the plunging jet. Type 2 dispersions are a mixture of types 1 and 3 dispersions where the bubbles are entrained by a vortex around the jet. These three types of bubble dispersion regimes were identified by visualisation.

Most techniques used to measure the important characterisation parameters (e.g. gas hold-up, bubble size, etc.) of a plunging jet in the laboratory (e.g. photography, conductivity probes) would not be suitable for monitoring industrial applications, where visualisation of a dispersion and its individual bubbles is often impossible and the liquids involved can foul probes. Acoustic emission monitoring is relatively non-invasive and is a rapid measurement technique [4]. Within this paper, an investigation of the acoustic emissions from a plunging jet and the interpretation of these acoustic emissions to characterise the dispersion is presented.

Bubble formation is an acoustically noisy process. On its formation, a bubble oscillates emitting an acoustic pulse. The frequency of the acoustic pulse has been shown to be related to the size of the bubble (i.e. diameter) according to Eq. (3) [5,6].

$$f = \frac{1}{\pi d}\sqrt{\frac{3\gamma p_0}{\rho}} \tag{3}$$

where f is the frequency of the pulse, d the diameter of the bubble, p_0 the pressure of the external liquid, ρ the liquid density and γ is the adiabatic constant. There have been many acoustic studies in the area of entrainment of bubbles in the sea [7]. The acoustic emissions caused by bubble formation in processes relevant to the chemical industry have also been investigated [8,9]. Initially, Pandit et al. [8] related the bubble size distribution in a submerged gas–liquid jet to the resulting acoustic spectrum. Boyd and Varley [9] demonstrated that the acoustic emissions in a gas–liquid agitated vessel were due to bubble formation at the impeller and for a specific set of conditions related the bubble size distribution to the acoustic emission spectrum. By estimating the bubble size distribution from an acoustic spectrum, identification of individual bubble pulses in the time signal and counting them is not necessary.

Leighton et al. [10] measured the acoustic emissions of liquid jets (at flow rates between 0.3 and 3.2 L min^{-1}) from a 5 mm nozzle impacting on a surface, after being ejected upwards at an angle, and entraining bubbles. A Gabor transform time-frequency signal analysis technique was used to determine bubble size and to count entrained bubbles. The bubble size distributions were found to be multi-modal and generally did not fit the proposed break-up models. Entrainment was found to decrease with decreasing jet flow rate and with the angle of the jet. Peaks in the bubble density distribution occurred at 2 kHz, which would, according to Eq. (3), correspond to a bubble of approximately 3 mm in diameter oscillating at its natural frequency. A peak in the distribution at 700 Hz was also observed especially at high entrainment rates and this corresponds to a bubble of approximately 9 mm in diameter; bubbles of this size were not observed in photographs. The 700 Hz peak could therefore possibly correspond to collective oscillations of the bubble dispersion. Mannaseh and Chanson [11] have also used an acoustic pulse counting technique from bubble formation events in a plunging jet to produce a bubble size distribution but the effects of process conditions on the acoustic emissions and the resulting bubble size distribution were not discussed.

In this study, the characterisation of hydrodynamic parameters of plunging jets from their acoustic time signals and spectra is investigated. The onset of bubble entrainment can be detected from the occurrence of pulses in the acoustic time signal. The calibration technique developed by Boyd and Varley [9] for agitated vessels is applied to the plunging jet system and used to demonstrate the effects of jet flow rate, nozzle height and liquid properties on the bubble size distribution. The hydrodynamic regimes of a plunging jet were identified from the sound spectrum.

2. Experimental

2.1. Plunging jet system

Fig. 1 shows a schematic diagram of the experimental apparatus. An EHEIM 1250/Charles Austin pump was used to re-circulate liquid through a 0.6 m long, 5 mm diameter nozzle to create a jet, which plunged into a cylindrical bath 0.21 m in diameter and 0.40 m high. Liquid was filled to a height of 0.3 m. The liquid flow rate was controlled by a Platon flowmeter. Flow rates used ranged from 1.4 to 4.4 L min^{-1} and the corresponding jet velocities at the nozzle are shown in Table 1. The liquid was impacted onto the

Table 1
Liquid velocities at the nozzle for the flow rates used

Qw (L/min)	v_0 (m/s)
1.5	1.27
2	1.70
2.5	2.12
3	2.55
3.5	2.97
4	3.40
4.4	3.73

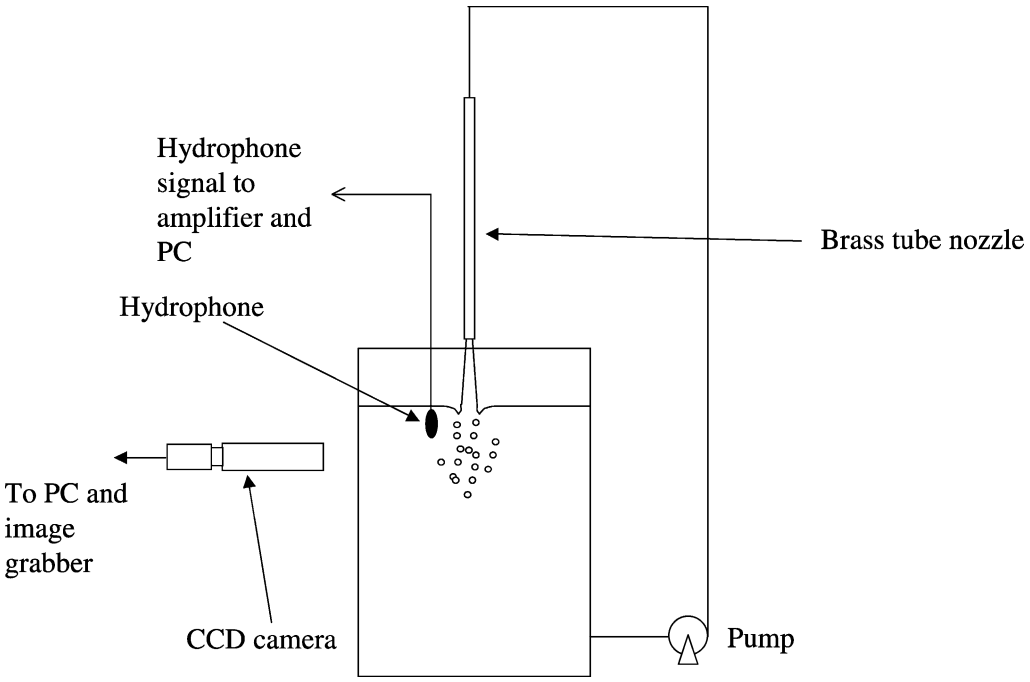

Fig. 1. Schematic diagram of plunging jet system.

liquid surface at an angle of 90° and the jet velocities at the liquid surface were calculated from Eq. (4).

$$v_j = (v_0^2 + 2gh_j)^{1/2} \quad (4)$$

where v_0 is the jet velocity at the nozzle and h_j is the nozzle height. Nozzle heights used ranged from 5 to 110 mm.

2.2. Acoustic measurement

A Bruel and Kjaer 8103 hydrophone attached to a rod and positioned inside the liquid bath was used to measure the acoustic emissions of the jet. The signal from the hydrophone was amplified by a 2 channel Nexus 2692 conditioning amplifier with an analogue bandpass filter between 0.1 and 100 kHz. The amplified signal was then acquired to a PC using an NI 4551 dynamic signal analyser card (National Instruments, Newbury) at a sampling rate of 200 kHz and analysed using LABVIEW and MATLAB software.

2.3. Photographic measurement

A Panasonic GP-MF622E camera fitted with a monozoom lens was used to digitally photograph the entrained bubbles. The camera was focused on an area 0.15 m below the water surface in the central plane of the vessel to reduce distortion effects caused by the curvature of the vessel wall. The photographed bubbles were analysed using Image ProPlus (Media Cybernetics). A scale was also photographed in order to calibrate the photographic measurements. Photographed bubbles were assumed to be spheroidal with the third dimension taken to be the same as the largest dimension in the 2-dimensional photograph. The size of these spheroidal bubbles was characterised by the diameter of a spherical bubble of the same volume calculated using Eq. (5).

$$d_{eq} = \sqrt[3]{AB^2} \quad (5)$$

where A is the smallest chord length and B is the largest chord in the 2-dimensional photograph.

3. Results

3.1. Time signal analysis

The onset of gas entrainment is marked by the occurrence of pulses in the time signal, which are not present unless entrainment is taking place. Fig. 2a shows 1 s of the pressure–time signal measured by the hydrophone (1 cm away from the jet, just below the liquid–air surface) at a flow rate just above the minimum entrainment velocity (1.7 L min^{-1}) of a water jet for a nozzle height of 5 mm. In this example, the magnitudes of pulses range approximately from 5 to 30 Pa and occur at a rate of around 100 pulses per second. In Fig. 2b, a magnified pulse is shown. An individual pulse generally has the form of an exponentially, damped sinusoid. This type of pulse, which is caused by the formation of a bubble, has been observed in other acoustic measurements of gas–liquid mixing discussed in the introduction [7,9,10]. The frequencies of the pressure pulses that contribute to the acoustic spectra range from 4 to 80 kHz

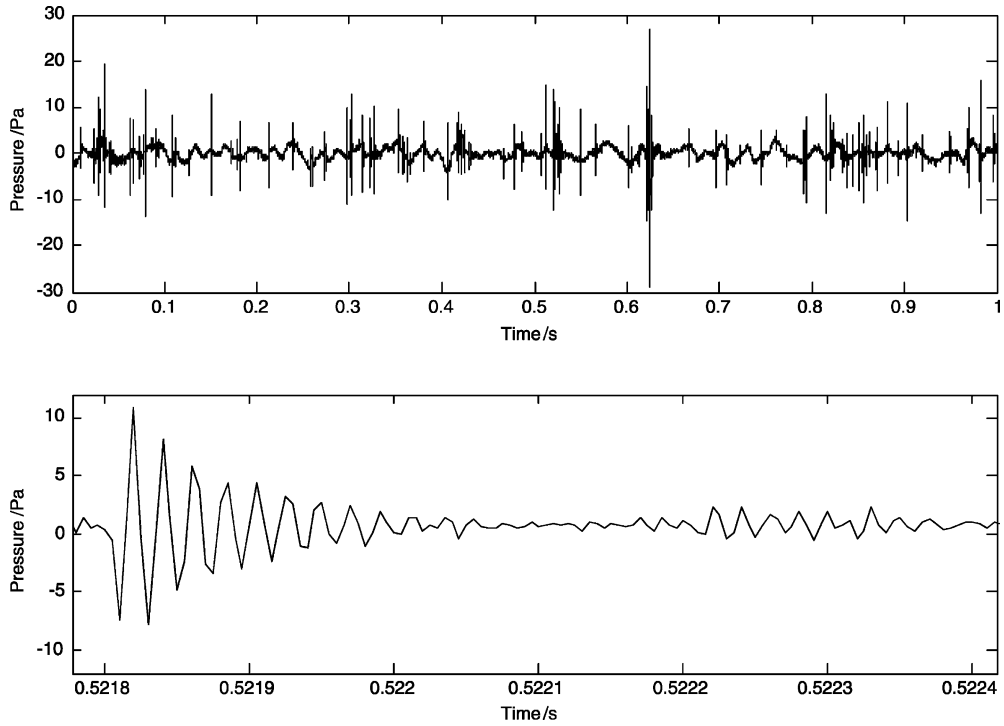

Fig. 2. Examples of bubble pulses highlighted in the measured time signals.

and these frequencies would correspond to bubble diameters of 1.6 mm down to 80 μm, respectively. Bubbles, approximately 2 mm in diameter and below, were visually observed at these corresponding process conditions.

In Fig. 3, three examples of pressure–time signals for increasing water jet velocities at a nozzle height of 5 mm are shown. The frequency at which the pulses occur within the time signals increases with increasing jet velocity due

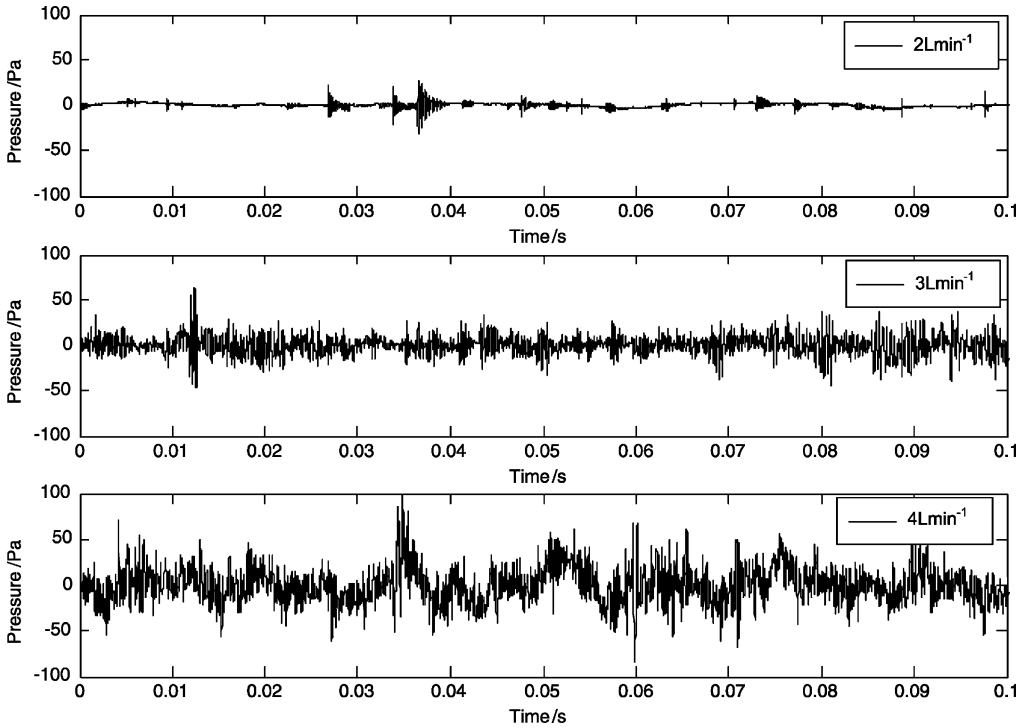

Fig. 3. The effect of increasing flow rate on the acoustic time signal.

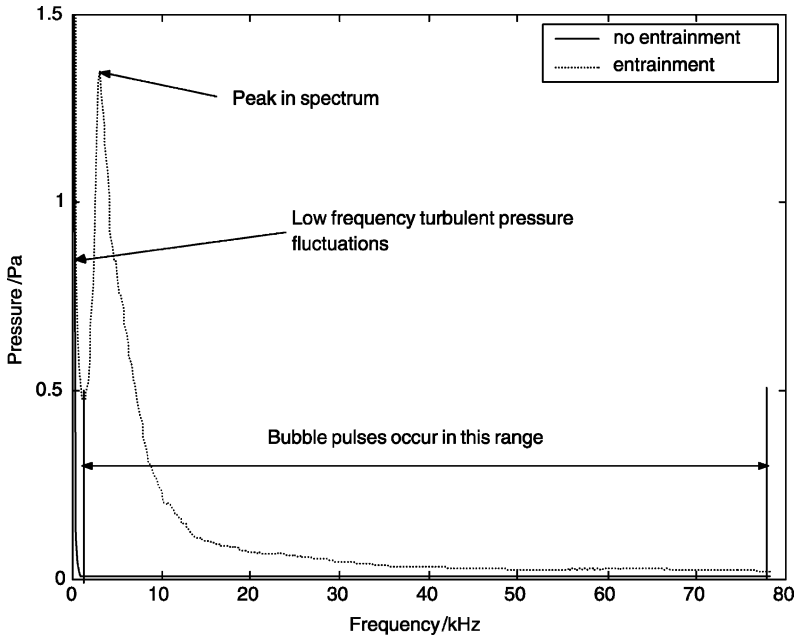

Fig. 4. Comparison of acoustic spectra with and without gas entrainment.

to an increase in bubble formation events and is likely to be due to greater entrainment and more break-up and coalescence events. At jet flow rates above 2 L min^{-1}, the bubble pulses begin to overlap making it increasingly difficult to identify pulses and their individual frequencies. The increased number of bubble pulses is due to increased entrainment and consequently more bubble formation events.

3.2. Spectral analysis and bubble size estimation

In Fig. 4, examples of two spectra are shown for conditions above and below the minimum velocity of entrainment (nozzle height of 5 mm and flow rates of 1.6 and 3 L min^{-1}, respectively) for the range of frequencies investigated in this study. Entrainment increases the pressure magnitude throughout the frequency range investigated. In both spectra, there is a low frequency range (below 600 Hz) where there is a contribution due to turbulent, hydrodynamic pressure fluctuations. In the case where entrainment occurred, the magnitude of the spectrum above 1 kHz is much higher than in the non-entrainment case and there is a peak at 5 kHz. Both the low frequency turbulence region and the high frequency bubble formation region have been observed in agitated tank measurements [9].

The effect of increasing jet velocity at a constant nozzle height (5 mm) on the acoustic spectrum is shown in Fig. 5a. The magnitude of the spectra in the frequency range due to bubble formation pulses increases with increasing jet velocity. This increase in spectral magnitude with jet velocity is the result of more bubble pulse events occurring as shown in the pressure–time data analysis (and possibly increased peak magnitudes due to more energetic bubble formation). A shift in the peak in the bubble pulse range to a lower frequency as the jet velocity increases suggests a shift of the maximum bubble size formed to larger bubble sizes and this concurs with visual observations of larger bubbles being formed at higher jet velocities. The spectra for the highest jet flow rate of 4 L min^{-1} show two peaks in the spectrum (peaks C and D), which suggests that there is a bimodal distribution of bubble pulse frequencies. Bimodal bubble size distributions have been observed in previous plunging jet entrainments [1].

An example of the effect of increasing nozzle height for a constant jet flow rate is shown in Fig. 5b. Increasing the height resulted in larger bubbles being observed and consequently a shift to lower frequencies in the spectra. Under certain conditions, the peak frequency was reduced to such an extent (at large nozzle heights and jet flow rates) that the bubble pulse range becomes indistinguishable from the turbulence frequency range.

Bubble size distributions have been estimated from acoustic spectra in previous studies [8,9]. The number of pulses, n_f, contributing to the acoustic spectrum at a frequency, f, is calculated by [8,9]:

$$n_f = \left(\frac{p_f^{\text{spec}}}{p_f^{\text{bubble}}} \right)^2 \tag{6}$$

where p_f^{spec} is the pressure magnitude of the spectrum at frequency f and p_f^{bubble} is the contribution of an individual bubble to the spectrum at frequency f. Clearly, an estimate of p_f^{bubble} is required before Eq. (6) can be applied. To do this theoretically requires knowledge of the bubble

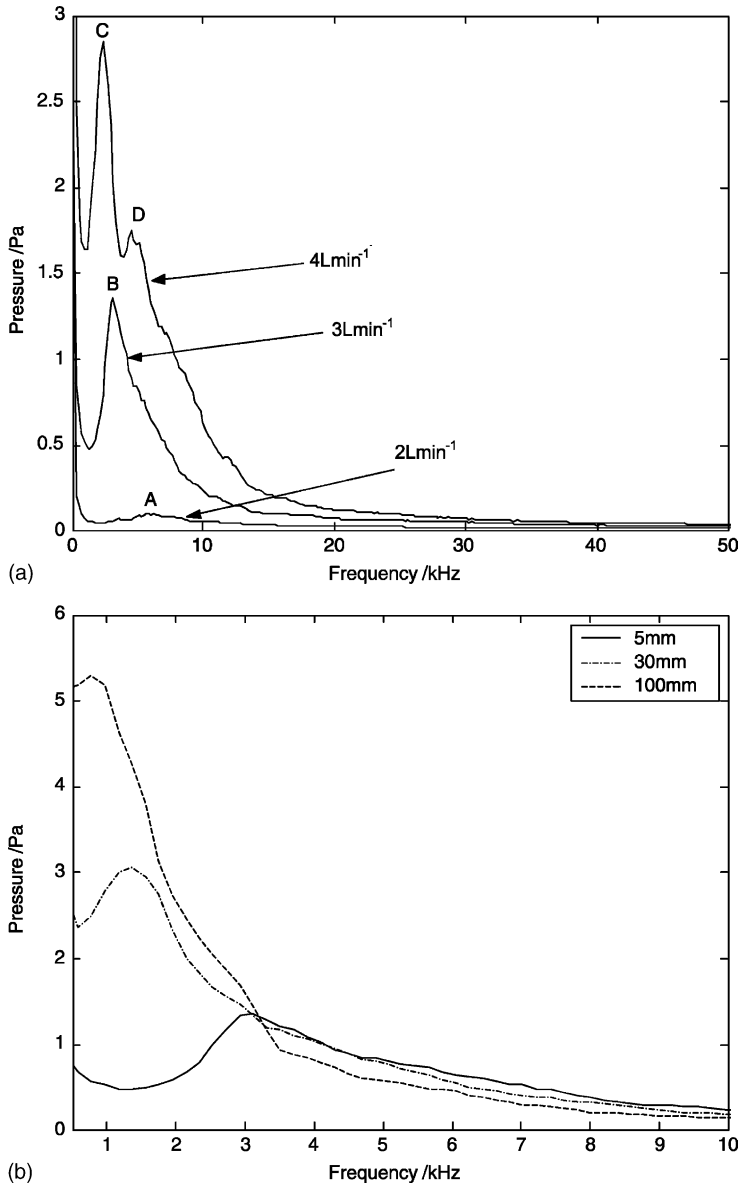

Fig. 5. Effect of (a) jet velocity and (b) nozzle height on the acoustic spectrum (note: the full frequency range of both spectra is up to 80 kHz.).

formation process. Pandit et al. [8] assumed that the initial change in bubble size was proportional to the size of bubble and therefore inversely proportional to frequency (using Eq. (3)) for a submerged gas–liquid jet. Boyd and Varley [9] empirically determined the peak magnitudes of the individual bubble formation pulses in an agitated vessel and used these to 'calibrate' the acoustic spectra so that the bubble size distribution could be calculated. For a nozzle height of 5 mm and water flow rate of 2 L min^{-1}, the pulse frequency distribution and the corresponding acoustic spectrum resulting from those pulses were measured; the results are shown in Fig. 6a and b, respectively. The average contribution of the individual pulses to the spectrum, p_f^{bubble} was calculated using Eq. (6) (unbroken line in Fig. 6c). The resulting calibration curve is shown in Fig. 6c. A curve fit of p_f^{bubble} with frequency (dotted line in Fig. 6c) resulted in:

$$p_f^{\text{bubble}} \propto \frac{1}{f^{0.9}} \tag{7}$$

with an $R^2 = 0.90$ which is close to the inverse relationship proposed by Pandit et al. [8] (where R is the correlation coefficient). Substitution of Eq. (7) into Eq. (6) gives the number of bubbles, n_f, at frequency, f, to be

$$n_f \alpha (p_f^{\text{spec}} f^{0.9})^2 \tag{8}$$

The fraction of bubbles, $\hat{n}_f$ at frequency, f, is given by

$$\hat{n}_f = \frac{(p_f^{\text{spec}} f^{0.9})^2}{\int_0^{80\,\text{kHz}} (p_f^{\text{spec}} f^{0.9})^2 \,\mathrm{d}f} \tag{9}$$

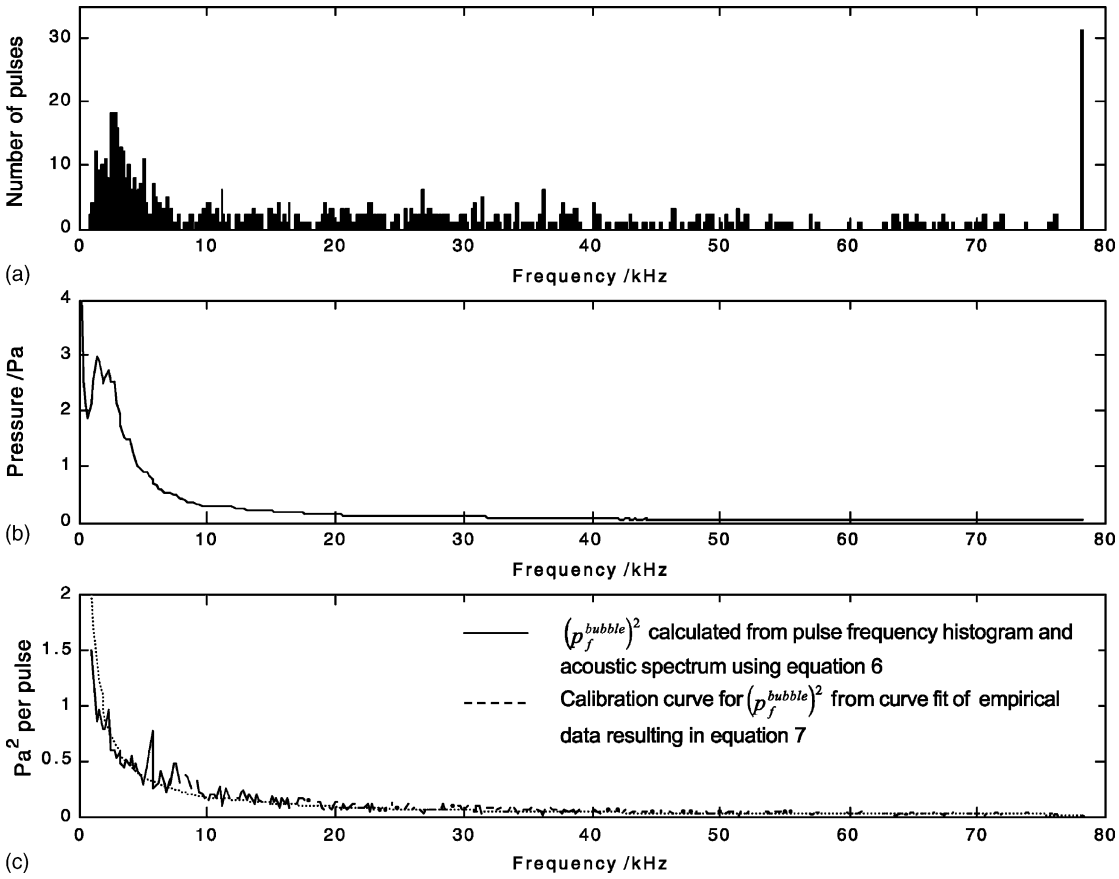

Fig. 6. Calibration of the acoustic spectrum for nozzle height of 5 mm and jet velocity of 2 L min^{-1}. (a) Histogram of pulse frequencies detected in a time signal (b) the resultant acoustic spectrum (c) empirically fitted calibration curve defined by Eq. (7).

The cumulative bubble size distribution is therefore given by

$$\tilde{N}(f) = \int_0^f \hat{n}_f \, \mathrm{d}f \tag{10}$$

The inverse relationship between bubble size and frequency means that the uniform distribution of frequency bins used to create the acoustic spectrum would result in a non-uniform distribution of bubble diameter size bins when constructing a bubble size histogram with the bin sizes increasing with increasing bubble size. As a consequence comparison with other distributions is difficult. A histogram of uniformly distributed bin sizes was estimated from the cumulative frequency distribution of pulse frequencies defined by Eq. (10) by defining a linear distribution of bin sizes and interpolating the values of in these bins. The $d_{\max}$ is defined as the diameter below which 99% of the bubble diameters in the cumulative distribution occur.

The mean diameter, d_m, is defined by

$$d_m = \frac{\sum_0^{d_{\max}} \hat{n}_{\mathrm{dia}} d_{\mathrm{bin}}^{\mathrm{mid}} \Delta d_{\mathrm{bin}}}{\sum_0^{d_{\max}} \hat{n}_{\mathrm{dia}} \Delta d_{\mathrm{bin}}} \tag{11}$$

where $\hat{n}_{\mathrm{dia}}$ is the fraction of bubbles in the diameter bin, $d_{\mathrm{bin}}^{\mathrm{mid}}$ the diameter bin mid-point and Δd_{bin} is the diameter bin width.

The Sauter mean diameter, d_{sm}, is defined by

$$d_{\mathrm{sm}} = \frac{\sum_0^{d_{\max}} \hat{n}_{\mathrm{dia}} (d_{\mathrm{bin}}^{\mathrm{mid}})^3 \Delta d_{\mathrm{bin}}}{\sum_0^{d_{\max}} \hat{n}_{\mathrm{dia}} (d_{\mathrm{bin}}^{\mathrm{mid}})^2 \Delta d_{\mathrm{bin}}} \tag{12}$$

In calculating the bubble size distributions the following assumptions were applied:

- The calibration curve defined by Eq. (8) applies for all jet flow conditions.
- Bubble formation was the only source of sound above 600 Hz (which would correspond to a 10 mm diameter bubble).
- A single bubble pulse at frequency, f, only contributes to the acoustic spectrum in the frequency bin at that frequency.

Fig. 7 shows the bubble size distributions of a plunging tap water jet at a nozzle height of 30 mm at flow rates of 2, 3 and 4 L min^{-1} calculated from the acoustic spectra as described above. The bubble size distribution shown for all three flow rates is bimodal. All three distributions have a peak at 0.35 mm and the majority of bubbles occur below 0.6 mm. This peak is likely to be caused by the formation of the primary bubbles initially entrained into vessel when the jet impacts onto the surface. A second, smaller peak occurs around

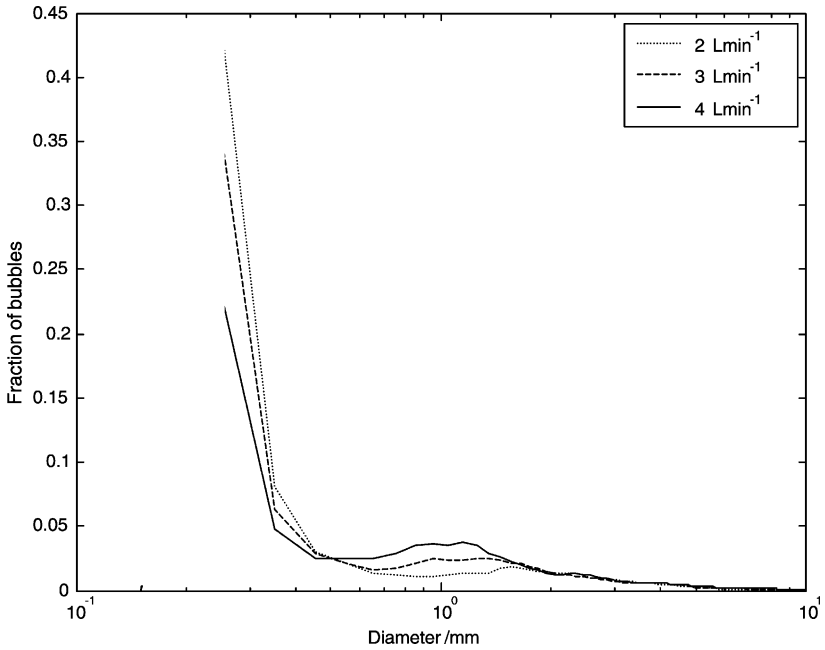

Fig. 7. Acoustically determined bubble size distributions at a nozzle height of 30 mm at different water flow rates.

1 mm and above. As the flow rate is increased, the fraction of primary bubbles within the dispersion decreases as indicated by the decrease in the height of the peak at 0.35 mm. The second peak in the distribution, which may be caused by the secondary bubbles formed by coalescence and break-up of the primary bubbles, shifts to the smaller diameters as jet flow rate increases. The likely explanation of this shift to smaller bubble diameters is the increase in turbulent energy resulting in greater bubble break-up. Also, the fractional number of these secondary bubbles increases with increasing velocity.

In Fig. 8, the variation of average bubble diameter, Sauter mean diameter and maximum bubble diameter with deionised water flow rate for a nozzle heights 2, 5, 10 and 50 mm is shown. For a particular nozzle height, the average bubble diameter initially increases with jet flow rate. At a certain flow rate, the increase in average bubble size ceases and the average bubble size remains approximately constant or decreases slightly with flow rate. The flow rate at which the increase in average bubble size plateaus or begins to decrease becomes lower as nozzle height is increased. Average bubble size is larger at increasing nozzle heights for the same jet flow rate. The maximum bubble size increases with flow rate (for the range of flow rates investigated) and as a consequence the Sauter mean diameter also increases with flaw rate even though the average diameter remains approximately the same above 3 L min^{-1}.

Iguchi et al. [12] presented a dispersion pattern map for a plunging jet system of the same geometry as used in these studies where the type of dispersion as defined by McKeogh and Ervine [3] was identified with flow velocity and nozzle height. A type 1 dispersion (small bubbles dispersed throughout the mixing vessel) can be clearly identified from the acoustically determined distribution, as there is not a second peak, which is present in the bimodal distributions of types 2 and 3 dispersions. Differentiating between types 2 and 3 dispersions acoustically measured distributions is more difficult because both are bimodal distributions and the exact point at which transition from a type 2 to type 3 dispersion is not dearly identifiable visually. The point at which the average bubble size begins to decrease with increasing jet flow rate could coincide with the transition from a vortex (type 2) to a turbulent (type 3) entrainment mechanism discussed by McKeogh and Ervine [3] where the increased turbulence results in greater bubble break-up.

Validation of this bubble size distribution technique is not a simple matter. Image analysis of photographs give a distribution at a single point and position at a specific time. The acoustic emissions from a gas–liquid dispersion are caused by the creation of bubbles (by entrainment, break-up and coalescence) at positions within detectable range of the hydrophone. An example of a photographically measured bubble size distribution is shown in Fig. 9 for comparison with a distribution estimated acoustically. Photographic techniques tend to only measure secondary bubbles [1] and as a consequence the photographic distribution is biased towards larger bubble sizes. The photographic bubble diameter distribution has peaks around 1 mm and has a maximum around 7 mm. In the acoustic distribution, most of the bubbles are below 0.5 mm in diameter with a small peak around 1 mm.

3.3. Effect of liquid physical properties

0.1, 0.2 and 0.3 M NaCl salt solutions were used to demonstrate the effect on the distribution of changing the

coalescence properties of the liquid. A 0.2 M NaCl solution is approximately at the critical concentration for coalescence (where coalescence rate is reduced by 50%) [13]. In Fig. 10, the calculated bubble size distributions from the acoustic spectra for deionised water, 0.1, 0.2 and 0.3 M NaCl are shown for a nozzle height of 10 mm and a flow rate of 3 L min^{-1}. In the previous section, it was proposed that the detected bubble size distribution is created through primary bubble formation (bubbles initially entrained at the surface) and secondary bubble formation (break-up and

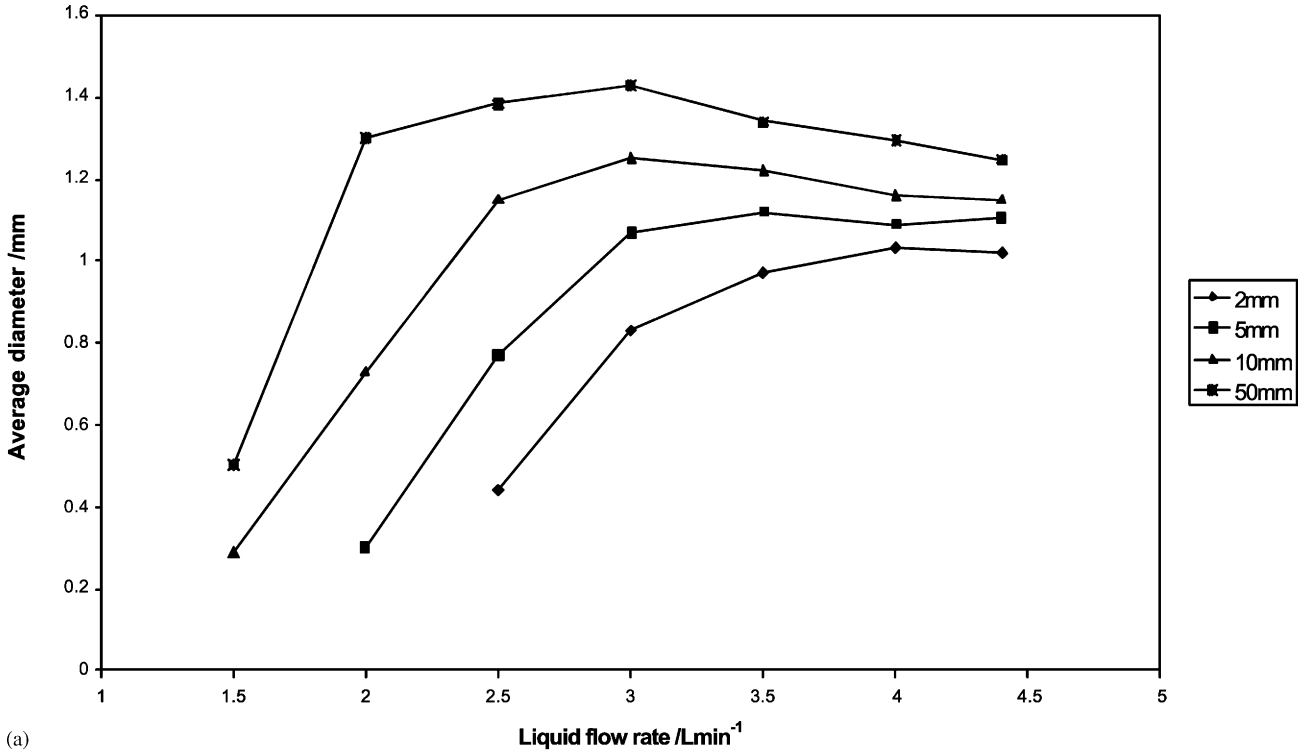

(a)

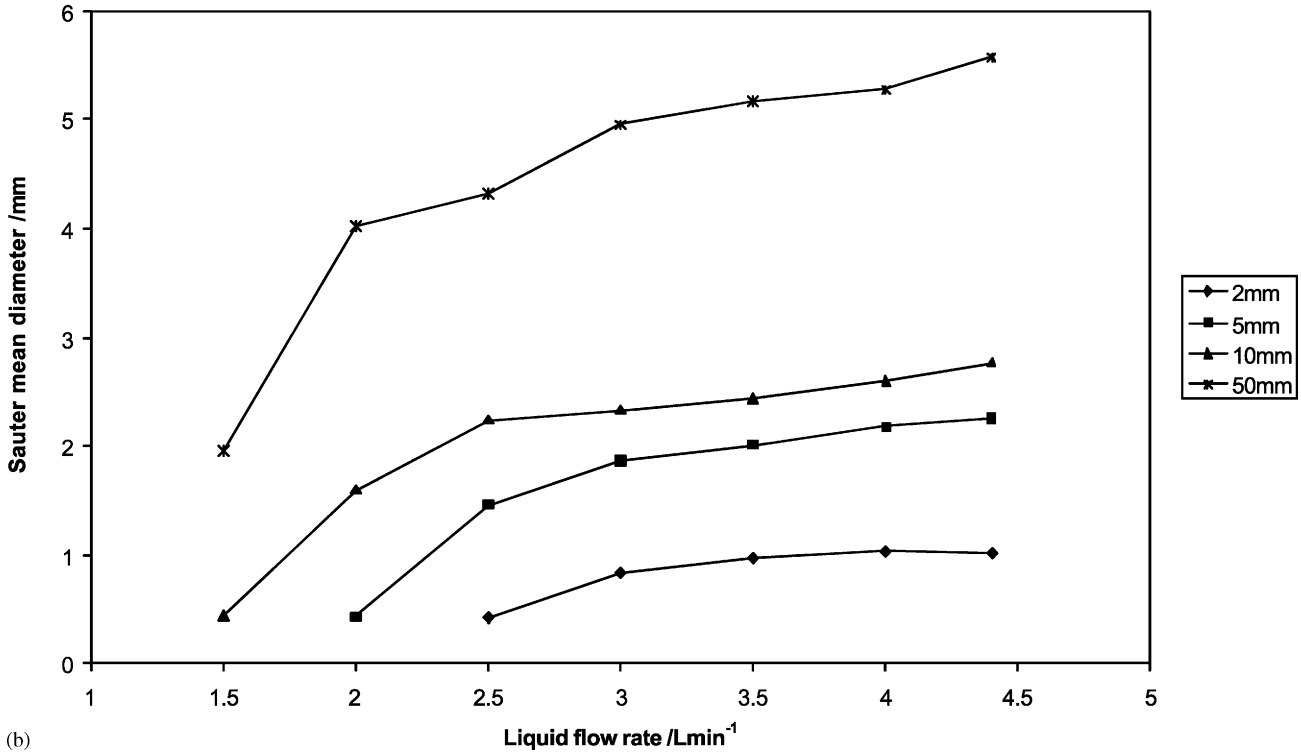

(b)

Fig. 8. The variation of average, Sauter mean and maximum bubble size in water with jet velocity at different nozzle heights.

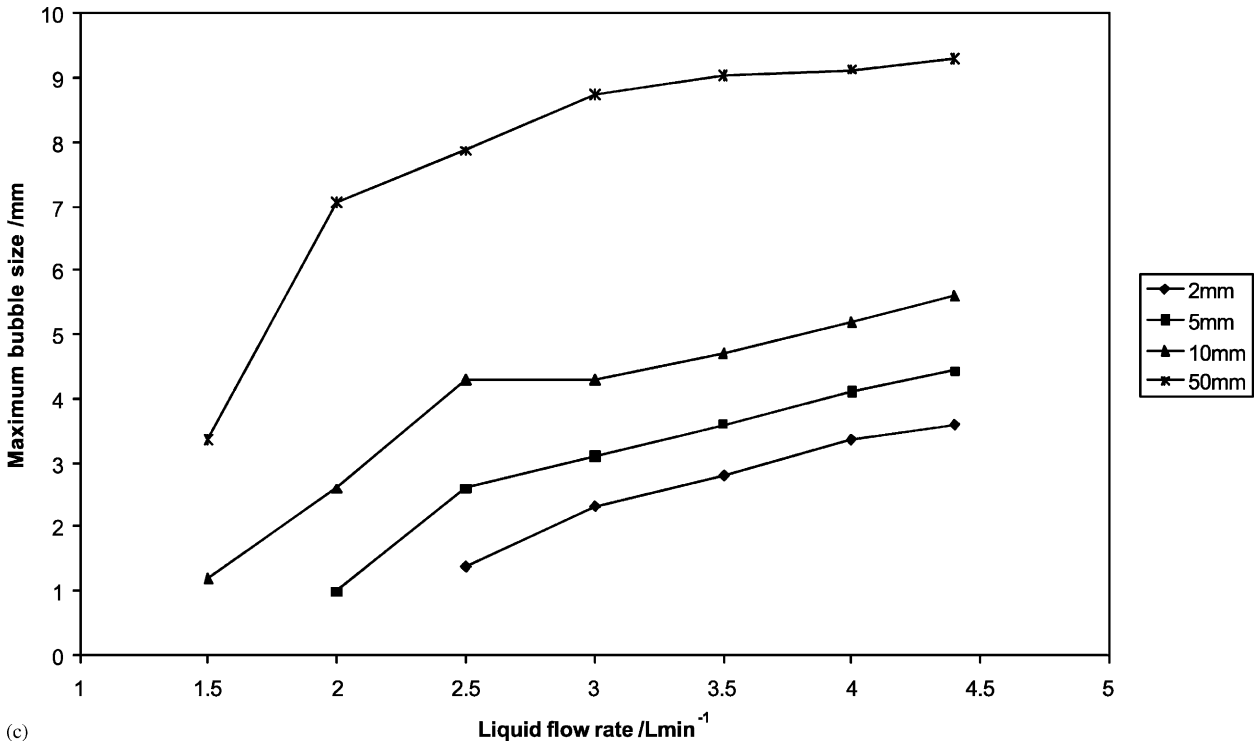

(c)

Fig. 8. (*Continued*).

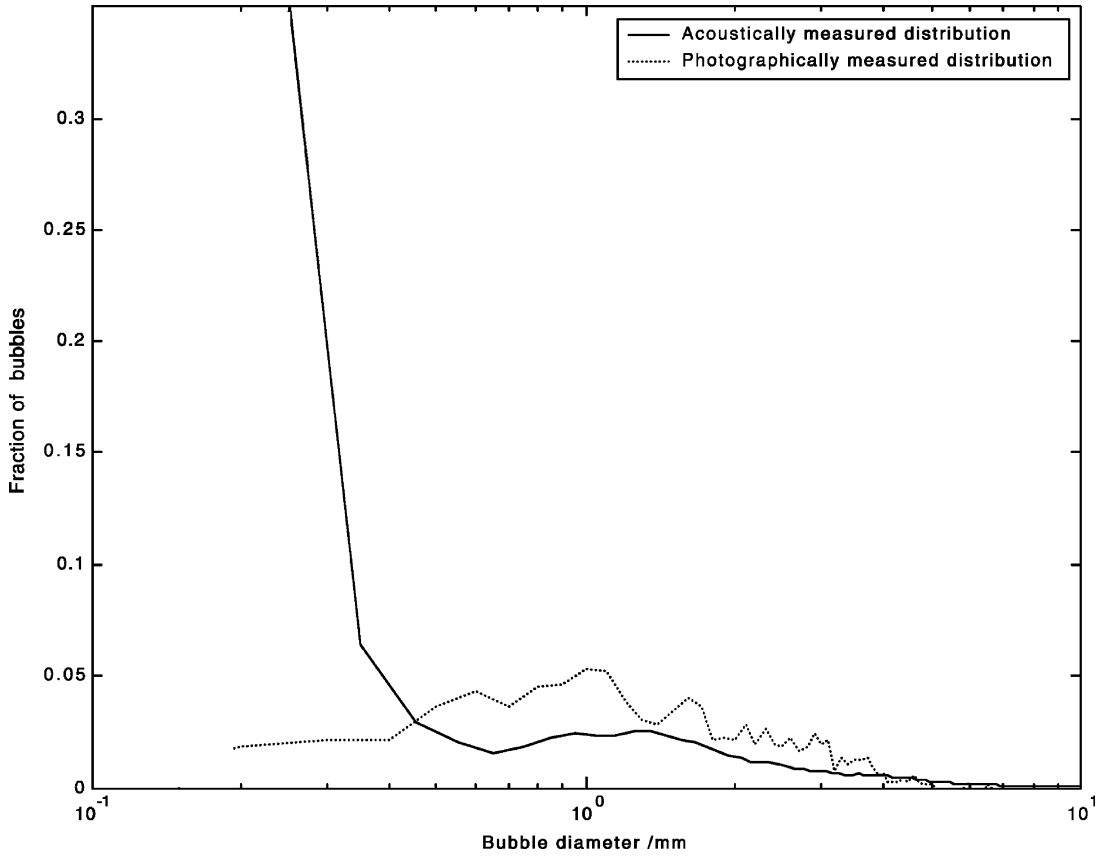

Fig. 9. Photographically measured bubble size distribution and an acoustically measured bubble size distribution for a water plunging jet with a nozzle height of 10 mm and a liquid flow rate of 3.0 L min^{-1}.

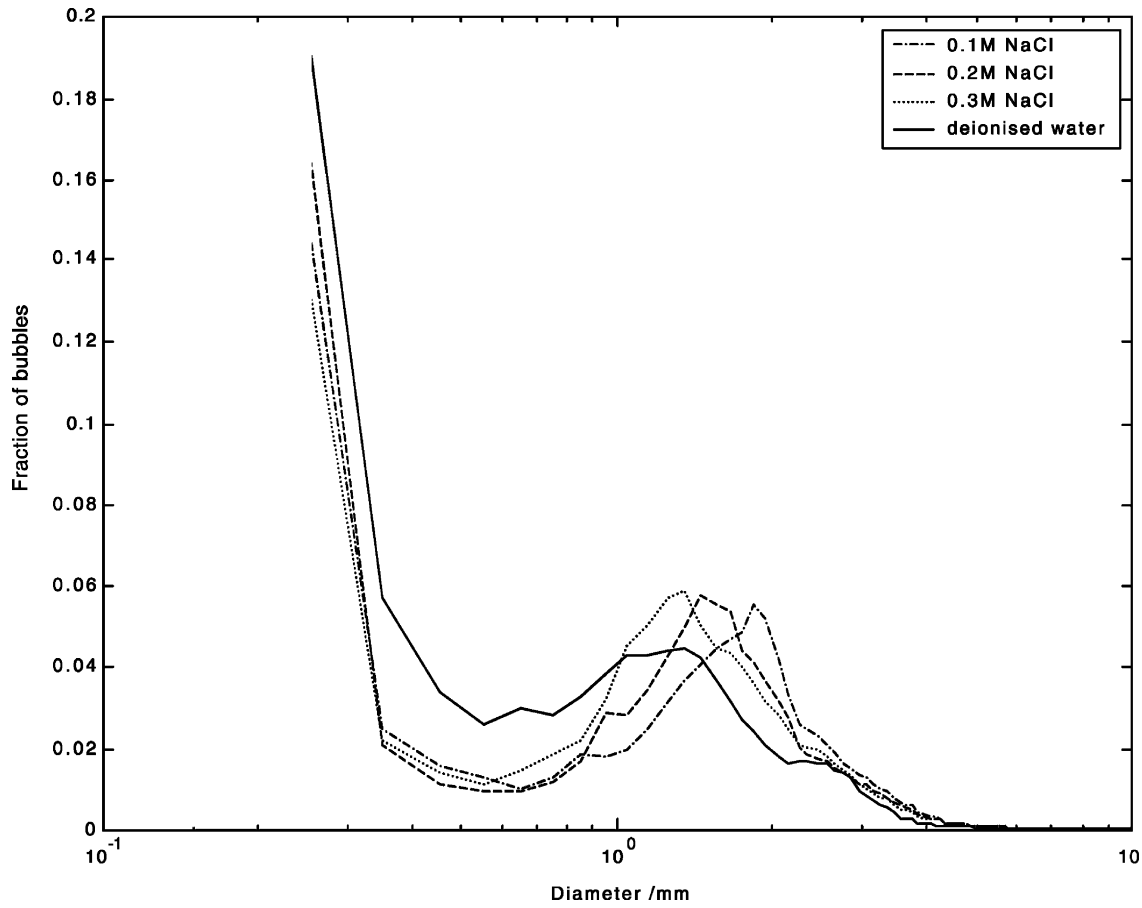

Fig. 10. Bubble size distributions at different salt concentrations for a nozzle height of 10 mm and a liquid flow rate of 3.0 L min^{-1}.

coalescence) and as a result, the distributions presented in Fig. 10 are bimodal. As the salt concentration is increased, the relative number of primary bubbles within the dispersion decreased. The relative number of the larger secondary bubbles within the dispersion increases with the salt concentration and there is a shift in the distribution of the peak of secondary bubbles to smaller sizes which suggests that break-up becomes the more dominant mechanism in secondary bubble formation.

How the above changes in the bubble size distributions due to changing NaCl concentration affect the average bubble size is shown in Fig. 11 where for three nozzle heights, the average bubble size calculated from the acoustic spectrum is plotted for different flow rates. The mean bubble sizes for deionised water for all nozzle heights and flow rates are always smaller than those in salt solutions. For a nozzle height of 5 mm, bubble diameter increases with liquid flow rate up to 3 L min^{-1} then remained approximately constant. In general, bubble diameters in 0.2 and 0.3 M solutions are approximately the same and larger than bubble diameters measured in 0.1 M solutions. For a nozzle height of 10 mm, again bubble size increases with increasing flow rate. The increase in bubble diameter levels off at 3.0 L min^{-1} for the 0.1 M and 0.2 M NaCl solutions whereas for the 0.3 M NaCl solution the increase in bubble diameter ceases at 2.5 L min^{-1}. The magnitude of bubble diameters in 0.1 and 0.2 M solutions is approximately the same but the diameters in 0.3 M NaCl are less than the magnitude of bubble diameters for the other solutions at flow rates of 3.0 L min^{-1} and above. At a nozzle height of 50 mm, salt concentration has a more severe effect on bubble diameter. 0.2 M NaCl solution produces the largest bubbles and 0.3 M solution the smallest. For all the salt solutions, bubble size increases with flow rate to a maximum then begins to decrease. For the lower nozzle heights of 5 and 10 mm, the salt concentration reduces the flow rate at which this decrease in bubble size occurs. At the higher nozzle height of 50 mm (Fig. 11C), the flow rate at which average bubble size begins to decrease remains approximately the same.

Previous studies of the effect of coalescence suppression in various gas–liquid systems using photographic or conductivity probe techniques [13,14] have indicated that bubble size decreases with increasing salt solution as coalescence is reduced. Therefore, bubble sizes as a result of gas entrainment from a plunging jet would be expected to decrease with increasing salt concentration. The acoustic determination of the average bubble sizes does not show this behaviour. The effect of increasing salt concentration clearly reduces the

bubble size of secondary bubbles as demonstrated by the shift in the peak of the secondary bubble range to the left.

However, the acoustically determined bubble size distribution is also the result of primary bubbles created by the impact of the jet on the liquid surface and the effect of salt concentration on this process is not clear. Measurement of the flow rate at which entrainment occurs at a constant nozzle height indicated that increasing salt concentration reduces

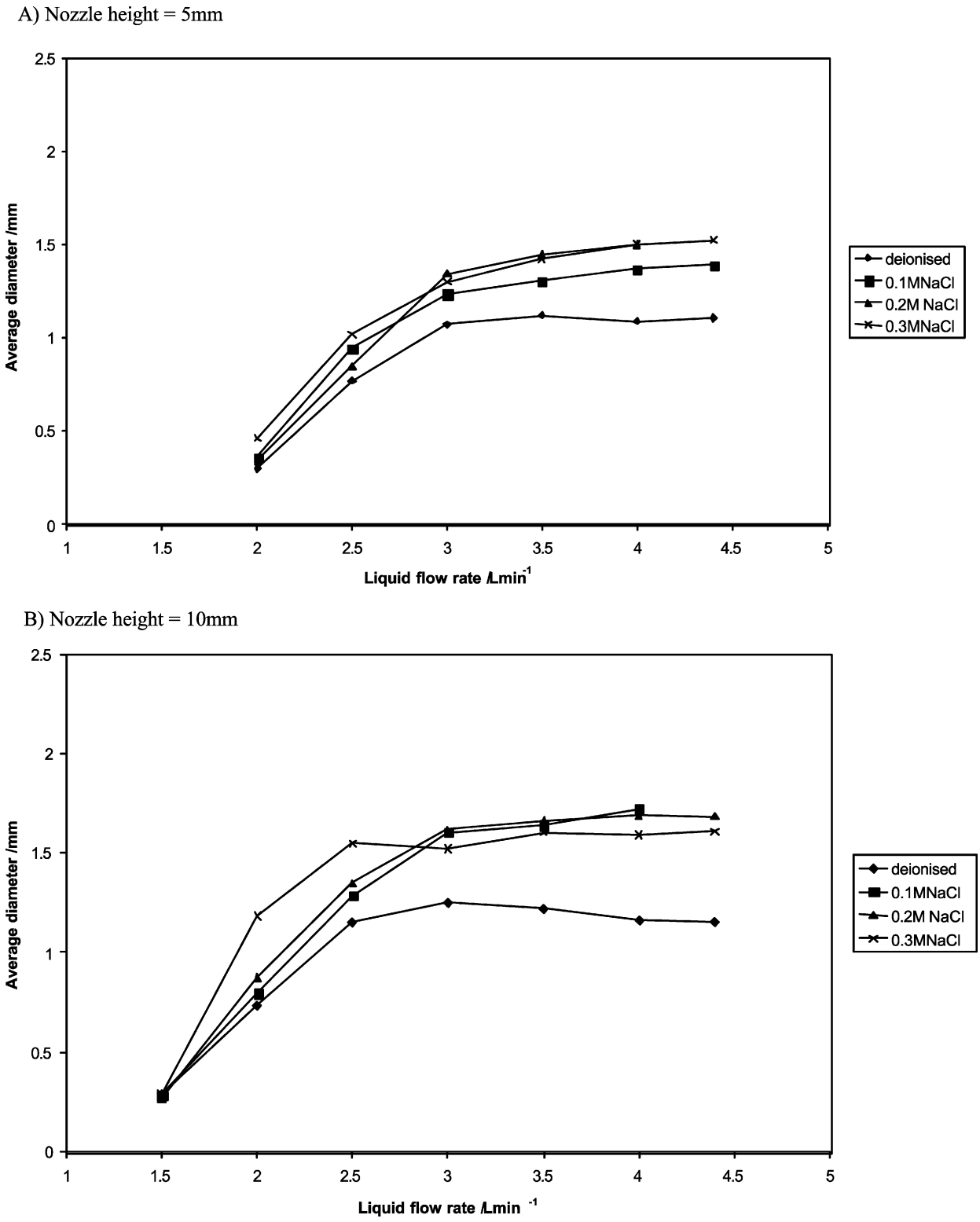

Fig. 11. The variation of Dm with jet velocity and height at different salt concentrations.

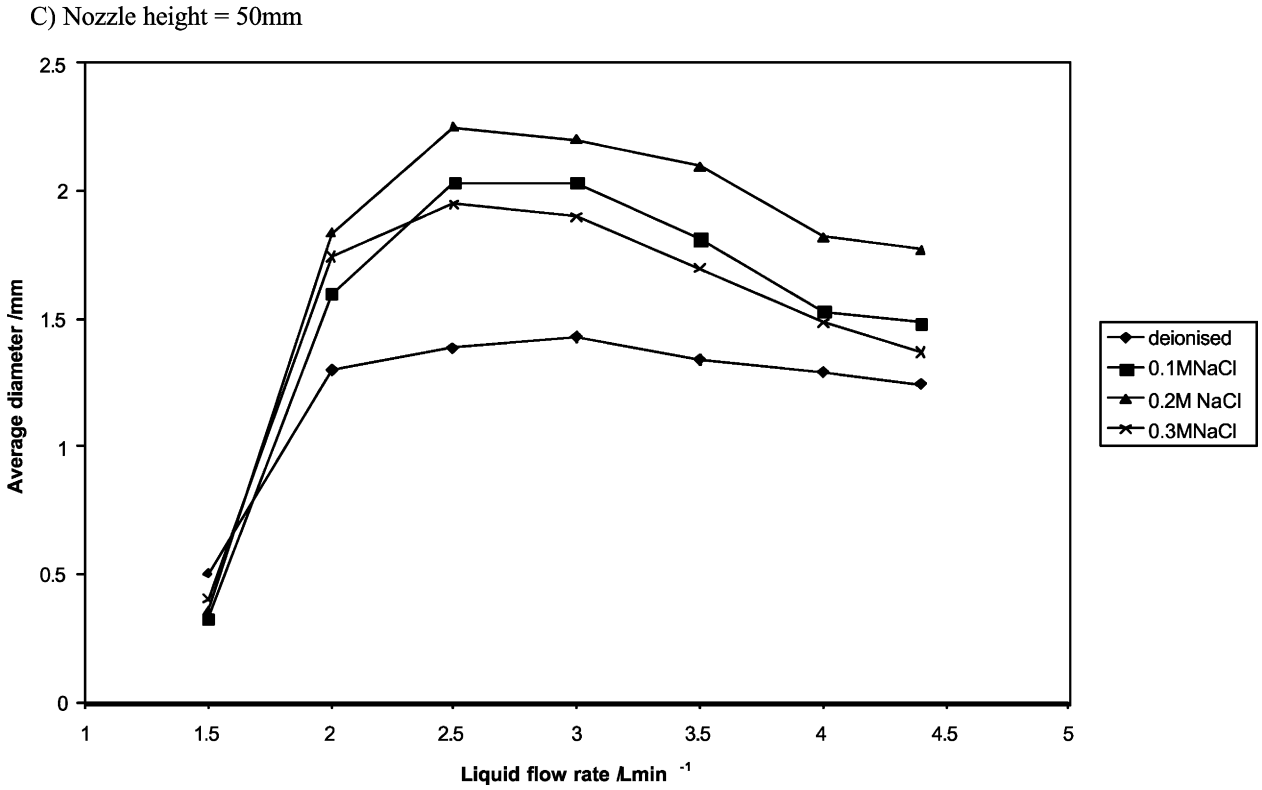

Fig. 11. (*Continued*).

the flow rate at which entrainment occurred and therefore at flow rates above the minimum entrainment flow rates, more gas and larger bubbles could be being entrained at the same jet flow rate for higher concentrations. However, Chanson et al. [15] found no change of the minimum flow rate for entrainment when comparing sea water, salt water (5.4 M NaCl) and tap water plunging jets but did detect a reduction in the void fractions with concentration, hypothesising that this was a result of the presence of salt 'hardening' the induction trumpet. Another possibility is that bubbles formed as a result of increasing the salt concentration are smaller than can be detected by the measurement system used in these acoustic studies. Clearly further investigation of this phenomenon is required.

0.01% and 0.05% xanthan gum solutions were used to demonstrate the effect of changing viscosity and for these two solutions the variation of average bubble size with flow rate for different nozzle heights is shown in Fig. 12. Xanthan gum solution is pseudoplastic in behaviour and its apparent viscosity, μ_a, is calculated using Eq. (13) [15].

$$\mu_a = K\dot{\gamma}^{n-1} \tag{13}$$

where $\dot{\gamma}$ is the shear rate and K and n are the consistency index and flow index, respectively and numerical values for the concentrations used in these studies taken from Miura and Kawese [16] are shown in Table 2. Increasing the concentration of xanthan gum will increase the viscosity of the system at the same shear rate. Shear rates will increase with increase with height and jet velocity. At the higher concentration of xanthan gum, shear rate will have an increased effect on viscosity due to a higher flow index. Therefore, at the higher concentration the effect of nozzle height and jet velocity will be more important as shear rates are increased. For a nozzle height of 5 mm there is very little difference in bubble diameter between the two different concentrations of xanthan gum and bubble size increases with increasing flow rate for both concentrations. At a nozzle height of 50 mm, bubble sizes are dramatically different with bubbles in 0.05% xanthan gum being approximately double the size of those in 0.01% xanthan gum. The effect of flow rate is similar for both concentrations, bubble size increasing with flow rate to a maximum then decreasing. The flow rate at which bubble size begins to decrease is lower for the 0.01% xanthan gum than for 0.05% xanthan gum (2.5 L min^{-1} as opposed to 3 L min^{-1}). If the nozzle height is increased further to 100 mm, initially at low flow rates the mean bubble sizes in the 0.05% xanthan gum solution are much higher than in 0.01% solution but for the 0.05% solution the mean

Table 2
Viscous and density properties for xanthan gum

Liquid	n	K (Pas^n)	ρ_l (kg m^{-3})
Water[a]	1	0.0009	997
Xanthan gum[a] (0.01 wt.%)	0.913	0.00246	997
Xanthan gum[a] (0.05 wt.%)	0.751	0.0166	998

[a] Taken from reference [16].

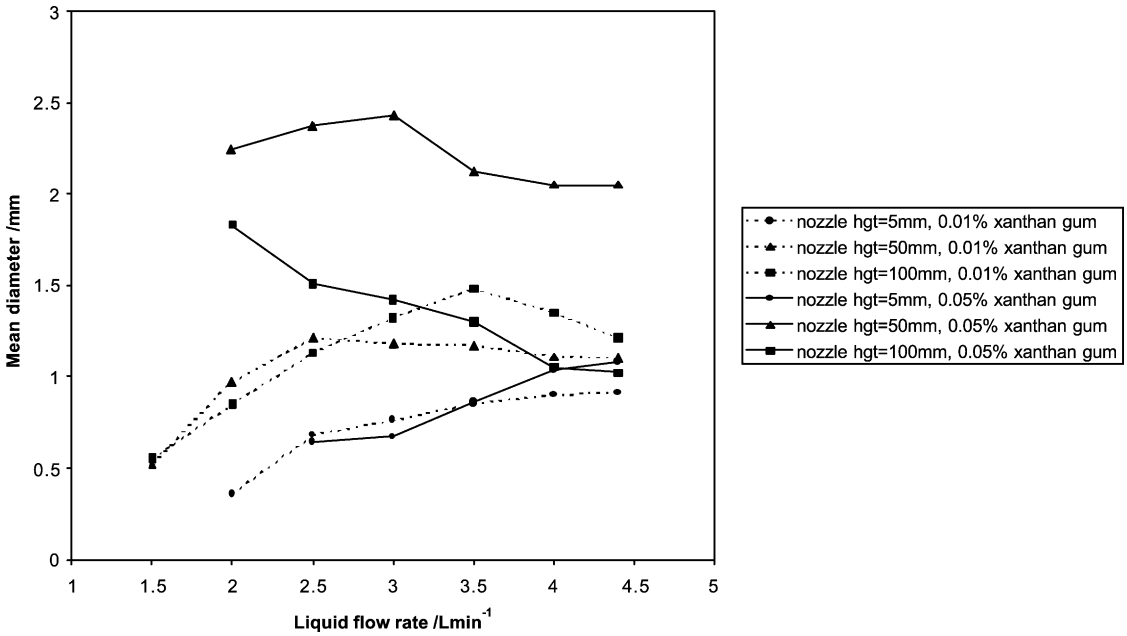

Fig. 12. The variation of Dm with jet velocity and nozzle height for 0.01 and 0.05% xanthan gum.

bubble sizes decreases with increasing flow rate. Flow rate has a similar effect on mean bubble size in 0.01% solution as at other nozzle heights; bubble size increases with flow rate initially then at 3.5 L min^{-1} decreases.

In calculating the distributions discussed above, it was assumed that the calibration curve of Eq. (7) is still applicable for the NaCl and xanthan gum solutions used. With the concentrations involved, the liquid density changes will have no significant effect on the frequency calculation of Eq. (3). NaCl concentration and viscosity will have an effect on the bubble dynamics and may therefore affect the calculations [17]. Further investigations of these effects are required to ascertain their significance in calculating the bubble size distribution.

4. Conclusions

The measurement of acoustic emissions from a laboratory scale plunging jet at low velocities was investigated as a means of monitoring key parameters and flow regimes non-intrusively and non-visually. The onset of bubble entrainment was identified from acoustic pulses due to bubble formation making the technique ideal for detecting entrainment in processes where entrainment is undesirable. The acoustic frequency was related to the bubble size and the effects of nozzle height and jet flow rate on acoustically determined bubble size distributions has been demonstrated. Bubble size distributions were found to be bimodal formed from small primary bubbles and larger secondary bubbles. For the low velocity range considered here, the mean bubble diameter increases with increasing flow rate to a maximum then decreases as turbulent break-up begins to dominate the bubble formation processes. Bubble dispersion regimes were identified from measured acoustic spectra. Different salt and xanthan gum solutions were used to demonstrate the effects of coalescence suppression and viscosity on the average bubble size and bubble size distribution estimated from acoustic measurement. Increasing salt concentration reduces the flow rate at which the average bubble diameter reaches a maximum with flow rate, suggesting turbulent break-up becomes the more dominant bubble formation process as coalescence is suppressed. The effect of xanthan gum concentration on bubble size becomes more important as nozzle height and jet flow rate in increased as a result of its pseudoplastic properties. Further investigation, however, is required to ensure the calibration of the acoustic technique is applicable to liquids of different physical properties.

Acknowledgements

The authors wish to thank the Royal Commission of the Exhibition of 1851 for Dr. Boyd's fellowship.

References

[1] A.K. Bin, Gas entrainment by plunging liquid jets, Chem. Eng. Sci. 48 (21) (1993) 3585–3630.
[2] G.M. Evans, G.J. Jameson, B.W. Atkinson, Prediction of the bubble size generated by a plunging liquid jet bubble column, Chem. Eng. Sci. 47 (13–14) (1992) 3265–3272.
[3] E.J. McKeogh, D.A. Ervine, Air entrainment rate and diffusion pattern pf plunging liquid jets, Chem. Eng. Sci. 36 (1981) 1161–1172.
[4] J.W.R. Boyd, J. Varley, The uses of passive measurement of acoustic emissions from chemical engineering processes, Chem. Eng. Sci. 56 (2001) 174–1767.

[5] M. Minnaert, On musical air-bubbles and the sounds of running water, Philos. Mag. 16 (1933) 235–248.
[6] T.G. Leighton, The Acoustic Bubble, Academic Press, London, 1994.
[7] A.R. Kolaini, L.A. Crum, Observations of underwater sound from laboratory breaking waves and the implications concerning ambient noise in the ocean, J. Acoust. Soc. Am. 96 (3) (1994) 1755–1765.
[8] A.B. Pandit, J. Varley, R.B. Thorpe, J.F. Davidson, Measurement of bubble size distribution: an acoustic technique, Chem. Eng. Sci. 47 (5) (1992) 107–1089.
[9] J.W.R. Boyd, J. Varley, Sound measurement as a means of gas bubble sizing in aerated agitated tanks, AIChemE J. 44 (8) (1998) 1731–1739.
[10] T.G. Leighton, P.R. White, M.F. Schneider, The detection and dimension of bubble entrainment and comminution, J. Acoust. Soc. Am. 103 (4) (1998) 1825–1835.
[11] R. Mannaseh, H. Chanson, Void fraction and acoustic characteristics of gas bubbles entrained by a circular plunging jet, in: Proceedings of the Fourth International Conference on Multiphase Flow, ICMF01, Paper 347, New Orleans, USA, 2001.
[12] M. Iguchi, K. Okita, F. Yamamoto, Mean velocity and turbulence characteristics of water flow on the bubble dispersion region induced by plunging water jet, Int. J. Multiphase Flow 24 (4) (1998) 523–537.
[13] V. Machon, A.W. Pacek, A.W. Nienow, Bubble sizes in electrolyte and alcohol solutions in a turbulent stirred vessel, Trans. AIChemE J. 75A (1997) 339–348.
[14] J. Zahradnik, M. Fialova, V. Linek, The effect of surface active additives on bubble coalescence in aqueous media, Chem. Eng. Sci. 54 (1999) 4757–4766.
[15] H. Chanson, S.-I. Aoki, A. Hoque, Scaling bubble entrainment and dispersion in vertical circular plunging jet flows: freshwater versus seawater, in: Proceedings of the Fifth International Conference on Hydrodynamics, Taiwan, 30 Oct–2 Nov 2002.
[16] H. Miura, Y. Kawese, Minimum liquid fluidization velocity in two and three phase fluidised beds with non-Newtonian fluids, Powder Technol. 97 (1998) 124–128.
[17] A.R. Kolaini, Sound radiation by various types of laboratory breaking waves in fresh and salt water, J. Acoust. Soc. Am. 103 (1) (1998) 300–308.